[CANCER RESEARCH 61, 4425–4431, June 1, 2001]

Isotype-specific Ras·GTP-Levels Predict the Efficacy of Farnesyl Transferase Inhibitors against Human Astrocytomas Regardless of *Ras* Mutational Status[1]

Matthias M. Feldkamp, Nelson Lau, Luba Roncari, and Abhijit Guha[2]

Arthur and Sonia Labatt Brain Tumor Research Centre, The Hospital for Sick Children, M5G-1X8 [M. M. F., N. L., L. R., A. G.]; Samuel Lunenfeld Research Institute, Mount Sinai Hospital, M5G-1X5 [M. M. F., N. L., L. R., A. G.]; Division of Neurosurgery, Toronto Western Hospital, University Health Network, and University of Toronto, M5T-2S8 [M. M. F., A. G.]; and Department of Surgical Oncology, Ontario Cancer Institute/Princess Margaret Hospital, M5T-2S8 [A. G.], Toronto, Ontario, Canada

ABSTRACT

Previous studies have demonstrated that astrocytomas express elevated levels of activated Ras·GTP despite the absence of activating *Ras* mutations. Farnesyl transferase inhibitors (FTIs) exert their antitumor effect in part through inhibition of Ras-mediated signaling. SCH66336 is a potent FTI presently undergoing clinical trials in patients with solid tumors. We evaluated the efficacy of SCH66336 against a panel of eight human astrocytoma cell lines and three human astrocytoma explant xenograft models in NOD-SCID mice. SCH66336 demonstrated variable antiproliferative effects against the cell lines, with IC_{50} ranging from 0.6 μM to 32.3 μM. Two of the three human glioblastoma multiforme (GBM) xenografts demonstrated substantial growth inhibition in response to SCH66336, with up to 69% growth inhibition after 21 days of treatment. Drug efficacy could be accurately predicted using a combination of the H-, K-, and N-isotype-specific Ras·GTP levels. These data indicate that the absence of *Ras* mutations does not preclude chemotherapeutic efficacy by FTIs, that Ras is likely a major target of FTIs regardless of *Ras* mutational status, and that isotype-specific Ras·GTP levels are a promising marker of drug efficacy.

INTRODUCTION

Activated GTP-bound Ras is a potent activator of intracellular signaling pathways, and its vital role is exemplified by the presence of oncogenic (activating) *Ras* mutations in approximately 25% of human malignancies (1). Inactive Ras·GDP is activated to the GTP-bound form by numerous upstream activators, and Ras·GTP is rapidly inactivated to Ras·GDP through an intrinsic GTPase activity catalyzed by p120-GAP and neurofibromin (2, 3). Oncogenic/activating *Ras* mutations lock Ras in its GTP-bound form (4), resulting in malignant transformation (5). Such activating mutations have not been identified in human astrocytomas, including the most malignant form, termed GBM[3] (1, 6). However, these tumors are characterized by the overexpression of ligand-dependent and -independent growth factor receptors (7–13). We have demonstrated in previous studies (14–16) that receptor-induced Ras activation is a common feature of GBMs and their derived cell lines, regulating both proliferative and angiogenic signals.

FTIs represent a promising novel class of molecularly targeted chemotherapeutic agents. These drugs inhibit the critical initial step in the post-translational modification of Ras (17, 18) and other farnesylated proteins (19). This step, catalyzed by farnesyl protein transferase, involves the transfer of a 15-carbon *trans,trans*-farnesyl moiety from farnesyl PP_i to the cysteine residue on the CAAX (C = cysteine; A = aliphatic amino acid; X = any other amino acid) motif at the COOH-terminal of Ras. Although initially intended to inhibit the proliferation of tumors in which the presence of oncogenic/activating *Ras* mutations resulted in persistently elevated levels of Ras·GTP, there is growing evidence that such agents also inhibit the proliferation of human cancer cell lines lacking such mutations (20–22); *e.g.*, we have demonstrated recently (22) that the FTI L-744,832 can inhibit the growth of established GBM cell lines by reducing cell cycle progression through both G_1-S and G_2-M, as well as by inducing apoptosis, even under anchorage-dependent conditions. Furthermore, L-744,832 potently inhibits the secretion of VEGF by these cells and, hence, may also demonstrate an antiangiogenic effect *in vivo* (22).

The FTI SCH66336 has recently completed Phase I clinical trials (23) with prior studies (24, 25) demonstrating promising effects against tumor cell lines in culture and in animal studies, although its efficacy against astrocytomas has not been reported previously. In the present paper, we demonstrate that SCH66336 decreases the viability of astrocytoma cells and inhibits the growth of human GBM explant xenografts in NOD-SCID mice. More importantly, we demonstrate that isotype-specific H-, K-, and N-Ras·GTP levels can accurately predict drug efficacy. These findings support the hypothesis that Ras is a major therapeutic target of FTIs even in tumors lacking oncogenic *Ras* mutations and that tumors with high levels of H-Ras·GTP are most sensitive to growth inhibition by these agents.

MATERIALS AND METHODS

Determination of Drug Efficacy against Human Astrocytoma Cell Lines. SCH66336 was obtained from Schering-Plough Research Institute (a gift of Dr. W. Robert Bishop, Kenilworth, NJ). SCH66336 is a novel trihalobenzocycloheptapyridine FTI (M_r, 638.8) modified from agents identified through a random drug screening program (26). U373 and U-343Cl2:6 cells were a gift of B. Westermark (Uppsala, Sweden); U118 cells were a gift of C. David James (Mayo Clinic, Rochester, MN); U138 and U87 cells were obtained from the American Type Culture Collection (Rockville, MD); and U251, SF763, and SF767 cells were a gift of Dolores Dougherty (University of California-San Francisco Brain Tumor Research Center). All of the cells were grown at 37°C in a 5% CO_2 incubator in DMEM supplemented with 10% calf serum. To measure cell viability, 1000 cells were plated in 96-well plates and treated with SCH66336 (1 nM-100 μM) for 10 days, with the number of viable cells determined using the Cell Titer 96 AQueous One Solution kit (Promega, Madison, WI; Ref. 27). Control cells were grown in medium alone or in medium supplemented with the vehicle (0.1% v/v DMSO). Dose-response curves were determined by modeling a log-normal dose-response relationship, with the IC_{50} defined as the dose at which the number of cells in the treatment well was 50% of that in control wells (Table 1).

Determination of Drug Efficacy against Human Explant Xenograft Models. NOD/SCID mice (NOD/LtSz-Prkdc^{scid}/J mice; Jackson Laboratory, Bar Harbor, ME) between 6–12 weeks of age were used to propagate human GBM explants obtained at craniotomy. Preliminary studies determined that the tumors grew more predictably in these mice than in BALB/c nude mice or SCID mice (data not shown). Pathologically verified GBM operative specimens were cut into approximately 2 × 2 × 2-mm fragments, and four to five pieces were implanted into the s.c. space of the right flank of each mouse.

Received 7/5/00; accepted 4/3/01.

The costs of publication of this article were defrayed in part by the payment of page charges. This article must therefore be hereby marked *advertisement* in accordance with 18 U.S.C. Section 1734 solely to indicate this fact.

[1] Supported by an operating grant from the National Cancer Institute of Canada (to A. G.). M. M. F. was supported by a Research Fellowship award from National Cancer Institute of Canada (provided in part by funds from the Terry Fox Run) and by a Research Fellowship from the Medical Research Council of Canada. A. G. is supported by a Clinician Scientist Award from the Medical Research Council of Canada.

[2] To whom requests for reprints should be addressed, at Division of Neurosurgery, Toronto Western Hospital, 399 Bathurst Street, Toronto, Ontario, Canada M5T 2S8. Phone: (416) 603-5740; Fax: (416) 603-5298; E-mail: Abhijit.Guha@uhn.on.ca.

[3] The abbreviations used are: GBM, glioblastoma multiforme; FTI, farnesyl transferase inhibitor; VEGF, vascular endothelial growth factor; IHC, immunohistochemical; HPβCD, hydroxypropyl-β-cyclodextrin; TUNEL, terminal deoxynucleotidyl transferase-mediated dUTP nick end labeling.

Table 1 *Total and isoform-specific Ras·GTP levels in astrocytoma cells and control rodent fibroblasts*

All of the Ras·GTP levels are normalized to total Ras·GTP levels in RT8 fibroblasts (positive control), which were given a value of 1.0 in each experiment. Actual IC_{50} levels (± 95% confidence limits) are those obtained through nonlinear regression of experimental data; predicted IC_{50} (± SE) are those predicted from the isotype-specific Ras·GTP levels by the regression model: IC_{50} (predicted) = 2.0 − 225.8[relative H-Ras·GTP] + 169.8[relative K-Ras·GTP] + 105.8[relative N-Ras·GTP].

	Ras·GTP (relative to RT8 cells)				IC_{50} (mm)	
Cell line	Total	H-Ras	K-Ras	N-Ras	Actual IC_{50} (±95% confidence interval)	Predicted IC_{50} (mean ± SE)
NIH3T3	0.011 ± 0.008	0.030	0.015	0.019		
RT8	1.000	1.240	1.207	1.365		
SF767	0.245 ± 0.208	0.042 ± 0.008	0.037 ± 0.004	0.015 ± 0.002	0.6 ± 0.1	0.42 ± 2.41
SF763	0.027 ± 0.019	0.018 ± 0.014	0.024 ± 0.021	0.018 ± 0.000	1.9 ± 0.2	4.10 ± 2.38
U251	0.197 ± 0.038	0.231 ± 0.061	0.218 ± 0.037	0.224 ± 0.034	5.6 ± 0.5	10.74 ± 2.49
U87	0.168 ± 0.054	0.181 ± 0.047	0.166 ± 0.039	0.134 ± 0.040	7.2 ± 0.9	3.46 ± 2.74
U118	0.186 ± 0.081	0.103 ± 0.030	0.083 ± 0.005	0.152 ± 0.065	11.3 ± 1.0	8.87 ± 3.10
U343	0.139 ± 0.046	0.139 ± 0.056	0.139 ± 0.052	0.156 ± 0.056	11.3 ± 1.0	10.75 ± 1.46
U138	0.128 ± 0.044	0.093 ± 0.000	0.123 ± 0.031	0.130 ± 0.024	15.0 ± 1.4	15.55 ± 2.06
U373	0.291 ± 0.030	0.261 ± 0.038	0.332 ± 0.073	0.301 ± 0.061	32.3 ± 1.5	31.27 ± 3.36

Three such xenografts (XEN01, XEN05, and XEN08) were used for this study, with IHC analysis of tumors from each passage confirming the maintenance of histological and molecular characteristics similar to the original human GBM tumor.

SCH66336 was dissolved in 20% w/v HPβCD and dosed at 50 mg/kg p.o. bid by oral gavage (volume, 100 μl), with the administered dose adjusted based on twice-weekly mouse weights. Vehicle-treated mice were provided with 20% HPβCD by twice-daily oral gavage. After the tumor volume ($V = a^2b/2$, where $a < b$) had reached approximately 200–250 mm^3, mice were randomized to receive either SCH66336 or HPβCD. The study was continued for 21 days, with twice-weekly mouse weight and tumor volume determination. Mice were sacrificed at the conclusion of the study, with portions of the tumor either flash-frozen in liquid nitrogen (to measure levels of Ras·GTP) or fixed in 10% buffered formalin (IHC analyses). Percentage growth inhibition {100 − [100 × (volume in drug group at day 21 − volume in drug group at day 0)/(volume in vehicle group at day 21 − volume in vehicle group at day 0)]} was calculated to determine the effect of SCH66336 on tumor growth (Fig. 1). The percentage growth inhibition was calculated twice weekly throughout the study, and the mean of these individual calculations was used to estimate the overall mean percentage growth inhibition. The growth fraction [1 − (percentage growth inhibition/100)] was calculated for use in the regression analyses.

Immunohistochemistry. Formalin-fixed, paraffin-embedded tissue sections from vehicle and drug-treated tumors were subjected to standard IHC analysis (Fig. 2). Primary antibodies were used to detect Ki-67 (polyclonal rabbit antibody #A0047; DAKO, Carpinteria, CA; used at 1:400), VEGF (polyclonal rabbit antibody #PU360-UP; BioGenex, San Ramon, CA; used at 1:400), and Factor VIII (rabbit polyclonal antibody #A0082; DAKO; used at 1:2500). Secondary antibody was a goat antimouse antibody (Zymed) used at 1:200, and antigens were detected using the avidin-biotin complex method (Vector Laboratories) and diaminobenzidine substrate. Apoptotic nuclei were detected using the TUNEL assay (28), and detection was performed according to the manufacturer's suggestions (*In Situ* Cell Death Detection kit-POD, Boehringer Mannheim).

Ras·GTP and Isotype-specific Ras·GTP Assays. A previously described (14, 29, 30) luciferase-based enzymatic technique was used to determine levels of activated Ras·GTP in both cells and in flash-frozen tissue specimens. This protocol was modified to determine isotype-specific Ras·GTP levels, with an additional immunoprecipitation step using a polyclonal antibody specific for H-Ras (sc-520) and monoclonal antibodies specific for K-Ras (sc-30) and N-Ras (sc-31; Santa Cruz Biotechnology, Santa Cruz, CA; Ref. 31). Lysates were immunoprecipitated with two of these isoform-specific antibodies for 1 h at 4°C, before subsequent immunoprecipitation with the neutralizing pan anti-Ras Y13-259 antibody (Oncogene Science), which locks Ras in either its GDP- or GTP-bound state; *e.g.*, H-Ras-specific Ras·GTP levels were determined from the supernatant of lysates precipitated with anti-K-Ras and anti-N-Ras antibodies. The affinity and specificity of the Ras isotype-specific antibodies were confirmed using lysates of cells overexpressing individual isotypes (a gift of Santa Cruz Biotechnology) and in experiments using astrocytoma cell and tumor lysates (Fig. 3). Total Ras·GTP, as well as H-, K-, and N-Ras-specific Ras·GTP levels were determined in duplicate from each

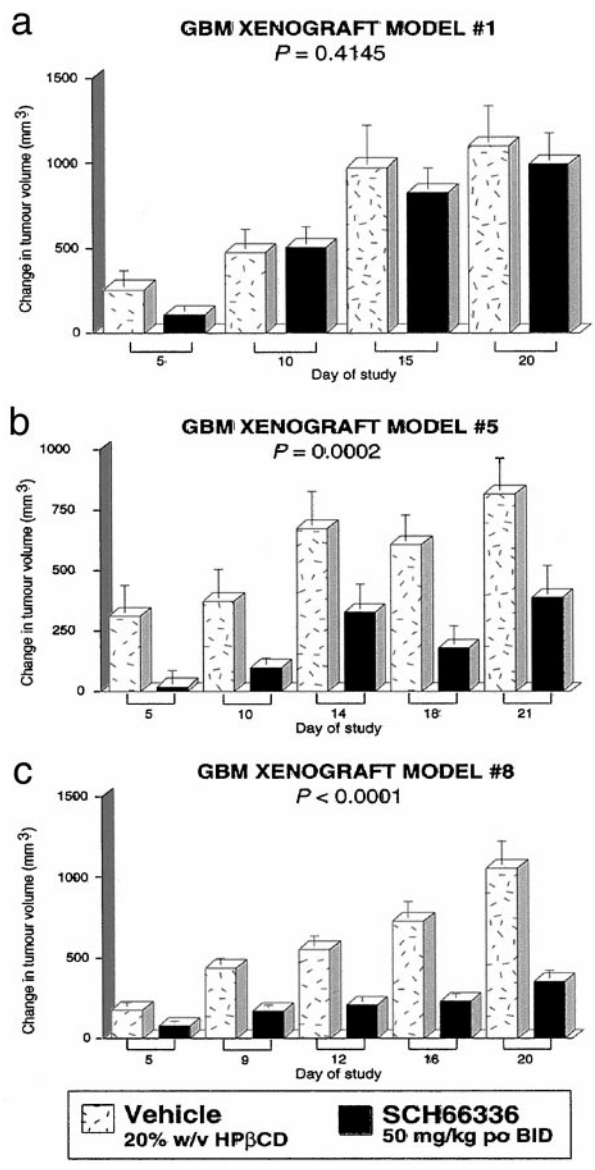

Fig. 1. Effect of SCH66336 on the growth of xenograft models was evaluated in NOD/SCID mice bearing s.c. flank XEN01, XEN05, or XEN08 GBM xenografts. Mice were dosed twice daily by oral gavage with either 100 μl of 20% w/v HPβCD or 50 mg/kg SCH66336 in a total volume of 100 μl of 20% w/v HPβCD. SCH66336 demonstrates relatively little antitumor effect against XEN01 xenografts, with a mean tumor growth inhibition of 19.4 ± 11.2% (*a*). In contrast, SCH66336 demonstrates significant antitumor effect against both XEN05 and XEN08 xenografts, with a mean growth inhibition of 68.7 ± 9.3% for XEN05 (*b*) and of 63.8 ± 5.0% for XEN08 (*c*).

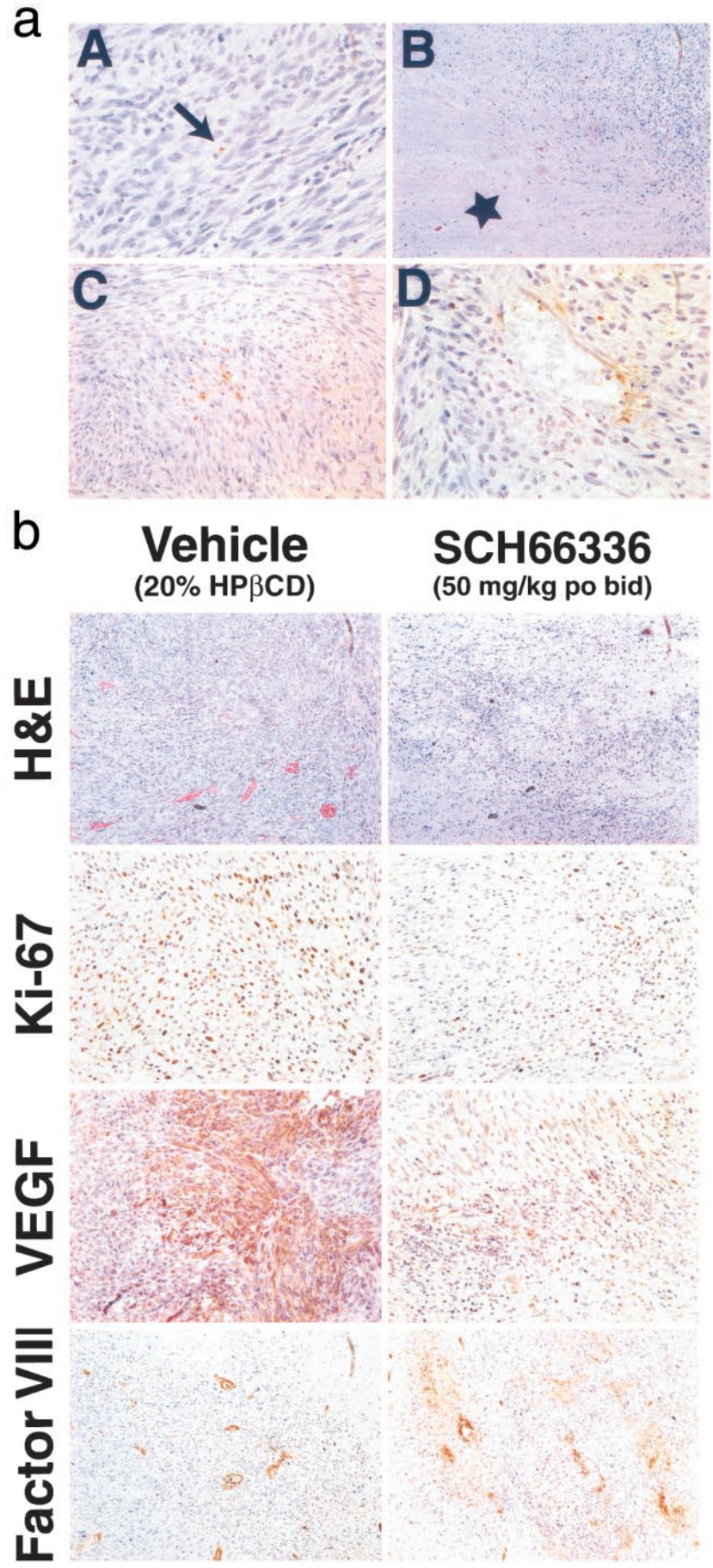

Fig. 2. *a*, photomicrographs of sections of xenograft GBM tumors (XEN08 model) from the s.c. space of NOD/SCID mice. *Top panels* are from vehicle-treated mice (*A* and *B*), whereas the *bottom panels* are from mice treated with 50 mg/kg p.o. bid SCH66336 (*C* and *D*). Vehicle-treated tumors demonstrate large regions of central necrosis (H&E staining; *B*, *star*; original magnification, ×100), with a virtual absence of TUNEL-positive cells within the solid portions of the tumor (*A*, *arrow*; original magnification, ×400). SCH66336-treated tumors were much smaller and demonstrate smaller regions of central necrosis but frequent regions of geographic necrosis throughout the tumor. Clusters of TUNEL-positive cells were seen throughout the drug-treated tumors (*C*; original magnification, ×200). A number of blood vessels in drug-treated tumors reveal TUNEL-positive cells within the vessel wall, suggesting an antiangiogenic effect of SCH66336 (*D*; original magnification, ×400), a feature that was not observed in the vehicle-treated tumors. *b*, photomicrographs of sections of xenograft GBM tumors (model XEN08) from the s.c. space of NOD/SCID mice. *Left panels* are from vehicle-treated mice, whereas the *right panels* are from mice treated with 50 mg/kg p.o. bid SCH66336 for 20 days. Sections were stained with H&E and probed for Ki-67, VEGF, and Factor VIII. Drug-treated tumors demonstrate an abnormal cytoarchitecture compared with vehicle-treated tumors (*H&E*). Both drug-treated and vehicle-treated tumors demonstrate the presence of Factor VIII-positive structures. These structures failed to form mature vascularized blood vessels in SCH66336-treated tumors (*H&E*). Vehicle-treated tumors demonstrate robust VEGF staining, even in solid tumor remote from the central necrosis, whereas drug-treated tumors demonstrate weak VEGF staining, even surrounding areas of necrosis. The Ki-67 labeling index appears uniformly high in vehicle-treated tumors, whereas in SCH66336-treated tumors, most of the tumor demonstrates very low or absent Ki-67 labeling. Original magnification, ×100 for H&E and Factor VIII; 200 × for Ki-67 and VEGF.

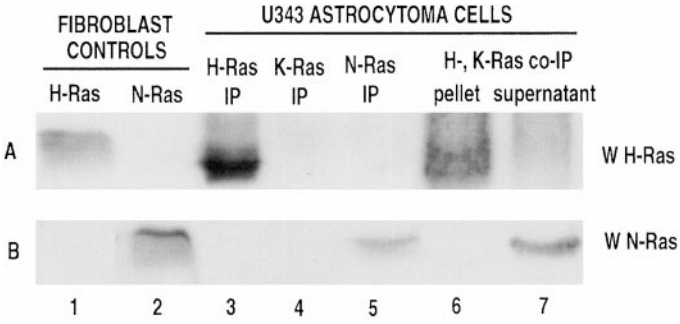

Fig. 3. Immunoprecipitation and Western blot analysis to determine the specificity of isotype-specific antibodies. Membranes were immunoprobed for H-Ras (*a*) and N-Ras (*b*). Fibroblasts overexpressing H-Ras demonstrate a strong band at M_r 21,000 when immunoprobed with anti-H-Ras but not anti-N-Ras (*Lane 1*), whereas the opposite pattern is seen for fibroblasts overexpressing N-Ras (*Lane 2*). *Lanes 3–5*, U343 astrocytoma cells immunoprecipitated only with anti-H-, anti-K-, or anti-N-Ras in single immunoprecipitation experiments. These studies demonstrate the specificity of these antibodies for immunoprecipitation and Western blotting. *Lanes 6–7*, the effect of double immunoprecipitations using U343 cells. Lysates immunoprecipitated with both anti-H- and anti-K-Ras demonstrate strong H-Ras expression in the pellet (*Lane 6*) and relatively little remaining H-Ras in the supernatant (*Lane 7*), whereas N-Ras is not detected in the pellet but is present in the supernatant. Similar results were obtained from xenograft lysates (data not shown). These studies thus demonstrate the ability of these double immunoprecipitation experiments to enrich the supernatant for the third Ras isotype.

sample. Because the isotype-specific Ras·GTP assays involve multiple antibodies and immunoprecipitation steps, total Ras·GTP is not simply a sum of the individual isotype-specific Ras·GTP levels. Therefore, all of the Ras·GTP levels were normalized to Ras·GTP levels in RT8 cells, and relative levels were used in all of the analyses (Tables 1 and 2).

Statistical Analysis. Data manipulation, ANOVA, and linear regression analysis were carried out using JMP version 3.2 (SAS Institute, Cary, NC). The IC_{50} of SCH66336 against the cell lines was determined by modeling a log-normal dose-response relationship using the probit function in SAS version 6.12 (SAS Institute). Drug efficacy in the xenograft models was determined using factorial ANOVA. The models predicting drug efficacy from isotype-specific Ras·GTP levels were constructed using forward stepwise regression analysis, in which individual variables are entered sequentially only if they improve the statistical validity of the model.

RESULTS

Efficacy of SCH66336 against Astrocytoma Cells and Human GBM Explant Xenografts. The IC_{50} of the eight GBM and high-grade astrocytoma cell lines tested are provided in Table 1. These IC_{50} were calculated after 10 days of treatment with SCH66336 and ranged from 0.6 μM for SF767 cells to 32.3 μM for U373 cells. The effect of SCH66336 on the xenografts was also variable (Fig. 1), with a nonstatistically significant growth inhibition (19.4 ± 11.2%; $P = 0.41$) for the XEN01 tumors ($n = 24$; 10 vehicle, 14 SCH66336; Fig. 1*a*). In contrast, SCH66336 had a statistically significant effect on XEN05 tumors ($n = 22$; 12 vehicle, 10 SCH66336), with a mean growth inhibition of 68.7 ± 9.3% ($P = 0.0002$; Fig. 1*b*). Consistent with this effect, the mean tumor weight of SCH66336-treated XEN05 tumors was 30.8% less than in vehicle-treated tumors after 21 days of treatment (1.88 ± 0.28 g for vehicle *versus* 1.30 ± 0.31 g for SCH66336; $P = 0.23$). Finally, SCH66336 demonstrated significant antitumor effects against XEN08 tumors ($n = 17$; 9 vehicle, 8 SCH66336), with a mean growth inhibition of 63.8 ± 5.0% ($P < 0.0001$; Fig. 1*c*). Drug-treated XEN08 tumors weighed 1.04 ± 0.19 g at harvest, compared with 1.88 ± 0.23 g for vehicle-treated tumors (a 44.9% reduction; $P = 0.0136$). HPβCD alone did not affect the growth of these tumors, in comparison with mice given 100 μl of drinking water twice-daily by oral gavage (data not shown; $n = 19$; $P = 0.88$).

IHC Analysis of SCH66336-treated Tumors. Formalin-fixed, paraffin-embedded sections from each GBM xenograft were subjected to IHC analysis. Vehicle-treated tumors grew very large, with extensive central necrosis (Fig. 2*a*, part *B*), a feature not found in the much smaller SCH66336-treated tumors. In contrast, the presence of TUNEL-positive tumor cells was unusual in vehicle-treated tumors (Fig. 2*a*, Part *A*) but was a common feature of SCH66336-treated GBMs (Fig. 2*a*, Part *C*). Individual blood vessels in drug-treated tumors revealed the presence of TUNEL-positive endothelial cells, suggesting an antiangiogenic effect that contributed to the overall decreased tumor growth in SCH66336-treated animals (Fig. 2*a*, part *D*). Apoptosis was not a feature of the tumor-associated blood vessels in the vehicle-treated GBMs (data not shown).

Viable regions of vehicle-treated tumors demonstrated extensive Ki-67 and bromodeoxyuridine labeling, many vascularized and Factor VIII-positive blood vessels, and robust VEGF expression by the tumor cells. In contrast, few components of drug-treated tumors were viable, with generally absent Ki-67 and bromodeoxyuridine labeling, a disorganized histological architecture, and weak VEGF expression (Fig. 2*b*). Both vehicle- and drug-treated tumors contained numerous Factor VIII-positive vascular structures. However, vehicle-treated tumors were well vascularized, with numerous red blood cells seen in H&E sections from these tumors. In contrast, drug-treated tumors lacked such evidence of vascularization (Fig. 2*b*).

Prediction of Drug Efficacy from Isotype-specific Ras·GTP Levels. Total and isotype-specific Ras·GTP levels were measured in all of the eight human malignant astrocytoma cell lines (Table 1). Total Ras·GTP levels did not help predict drug efficacy in the cell lines. Furthermore, H-Ras, K-Ras, and N-Ras isotype-specific Ras·GTP levels were relatively poor individual predictors of drug efficacy. However, forward stepwise multiple regression analysis demonstrated that the overall model comprised of the combination of H-, K-, and N-Ras·GTP levels was highly predictive of the IC_{50} ($R^2 = 0.9255$; $F = 16.5587$; $P = 0.0102$). As depicted in Table 1, the "predicted IC_{50}" from this regression analysis and derived from the overall model closely approximates the "actual IC_{50}" of the astrocytoma cell lines. As shown in Fig. 4, *a–d* (*top*), increasing K- and N-Ras·GTP levels predict for greater drug resistance, whereas increasing H-Ras·GTP levels predict for greater drug efficacy.

Table 2 *Total and isoform-specific Ras·GTP levels in human GBM tumors grown in NOD/SCID mice*

All of the Ras·GTP levels are normalized to total Ras·GTP levels in RT8 fibroblasts (positive control), which were given a value of 1.0 in each experiment. Actual growth fractions (± SE) are those determined from the animal experiments described in the text. Predicted growth fractions are those predicted from the isotype-specific Ras·GTP levels by the regression model: growth fraction (predicted) = 0.06 − 13.52[relative H-Ras·GTP] + 15.69[relative K-Ras·GTP] + 11.53[relative N-Ras·GTP].

	Ras·GTP levels (relative to RT8 cells)				Growth fraction	
Tumor sample	Total	H-Ras	K-Ras	N-Ras	Actual (mean ± SE)	Predicted (mean ± SE)
XEN01-A	0.052696	0.044931	0.044906	0.057279	0.806 ± 0.112	0.820 ± 0.020
XEN01-B	0.013454	0.031591	0.04019	0.045361		0.789 ± 0.018
XEN05-A	0.037782	0.052723	0.038629	0.030139	0.313 ± 0.093	0.303 ± 0.023
XEN05-1B	0.05314	0.053943	0.020921	0.056507		0.313 ± 0.022
XEN08-A	0.028342	0.035373	0.030648	0.027668	0.362 ± 0.050	0.384 ± 0.016
XEN08-B	0.027594	0.037049	0.024298	0.03574		0.355 ± 0.016

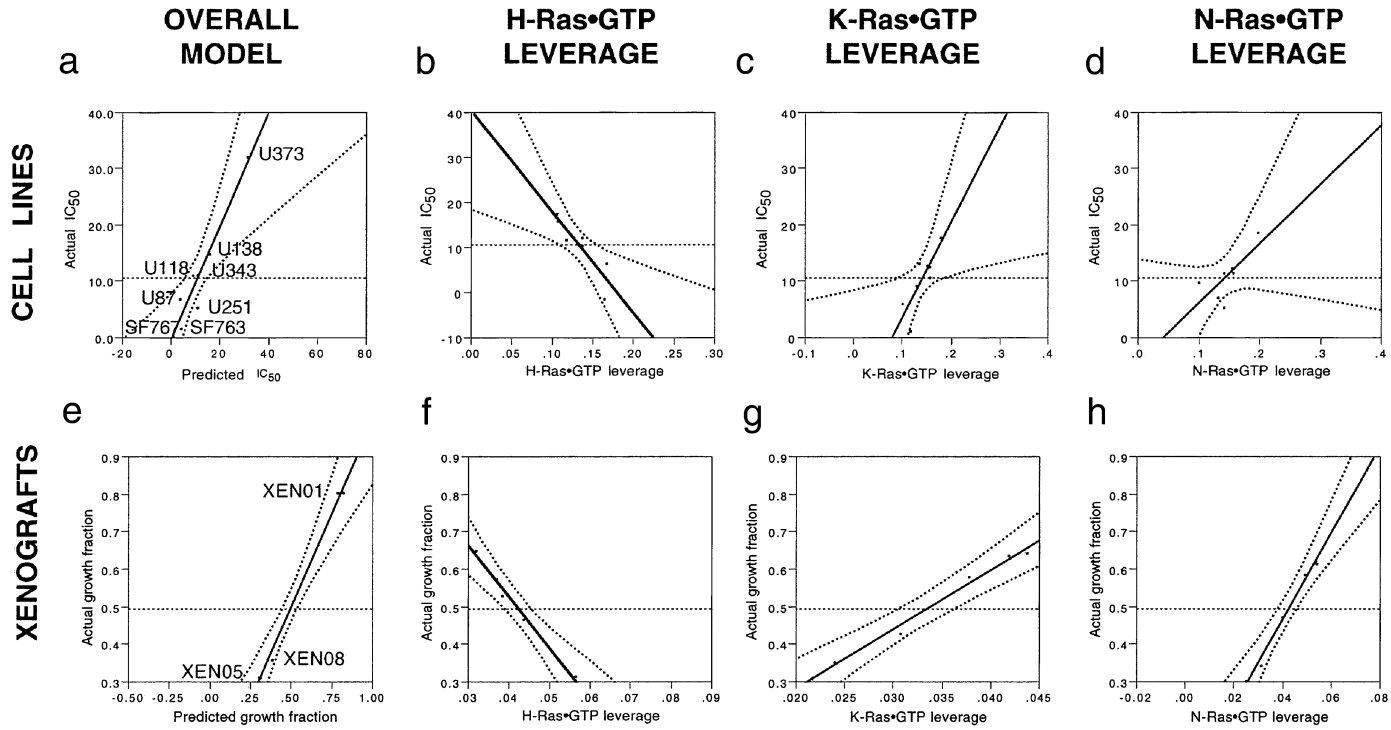

Fig. 4. Multiple linear regression was used to predict the IC_{50} for SCH66336 in a panel of eight astrocytoma cells (*a–d*), as well as the efficacy of SCH66336 against three GBM xenografts in NOD/SCID mice (*e–h*). To approximate the concept of an IC_{50}, in which higher levels imply greater drug resistance, the model for the xenografts predicts the growth fraction. The growth fraction is defined as the growth of drug-treated tumors in comparison with vehicle-treated tumors, with vehicle-treated tumors given a value of 1.0. The strongest regression model was constructed by excluding total Ras·GTP from the equation but by including each of the isotype-specific Ras·GTP levels. Predicted and actual IC_{50} levels were closely correlated in the cell lines (*a*; and Table 1), as were predicted, and actual growth fractions in the xenograft tumors (*e*; and Table 2). The *horizontal dashed line* in each graph represents the mean of all of the values. Leverage plots (*b–d* and *f–h*) depict the effect on residuals if that variable was removed from the model (49). These leverage plots demonstrate that increasing H-Ras·GTP levels correlate with increased drug sensitivity and reduced IC_{50}/growth fraction (*b* and *f*), whereas increasing K- or N-Ras·GTP levels correlate with increased drug resistance and increased IC_{50}/growth fraction (*c*, *d*, *g*, and *h*). *Dashed curves* around the regression line indicate the 95% confidence interval for each regression line.

Similar analyses were carried out for the human GBM xenograft models in NOD-SCID mice, with total and isotype-specific Ras·GTP levels measured from two tumors (denoted as A and B) from each of the three xenograft models (XEN01, XEN05, and XEN08; Table 2). To aid in the comparison of the cell line and xenograft data, IC_{50} was approximated in the xenografts by expressing drug efficacy as a growth fraction. The growth fraction was defined as the mean tumor volume increase over the course of the experiment in SCH66336-treated tumors in comparison with the mean volume increase in vehicle-treated tumors for each xenograft model. The volume increase in vehicle-treated GBMs was given a score of 1.0; thus, a growth fraction of 0.806 for SCH66336-treated XEN01 tumors is equivalent to a 19.4% growth inhibition. Regression analyses for these xenograft models yielded results similar to the cell lines. Neither total nor any of the individual isotype-specific Ras·GTP levels could independently predict drug efficacy; however, the overall model comprised of the combination of H-, K-, and N-Ras·GTP was strongly predictive of drug efficacy ($R^2 = 0.9962$; $F = 174.9624$; $P = 0.0057$). As depicted in Table 2, "predicted" growth fractions predicted on the basis of this regression analysis closely approximate the "actual" growth fraction of each of the tumors analyzed. Similar to the cell lines, increasing K- and N-Ras·GTP levels predict for greater drug resistance, whereas increasing H-Ras·GTP levels predict for greater drug efficacy (Fig. 4, *e–h*, *bottom*).

DISCUSSION

FTIs represent one of the first classes of antineoplastic agents designed through rational drug design. The high prevalence of activating *Ras* mutations in human cancers (1) initially suggested that approximately 25% of human malignancies may demonstrate sensitivity to such agents (32). However, two critical observations have made this prediction more complex. First, the presence or absence of *Ras* mutations does not appear to be the sole determinant of FTI efficacy, at least in cell lines (21). Second, *H-Ras*-transformed cells appear to be more sensitive to these agents than those transformed by either *K-Ras* or *N-Ras* (20, 31, 33, 34).

The first observation has cast doubts on whether Ras is a major therapeutic target of FTIs *in vivo*. This is because in addition to Ras, approximately 0.5% of all of the cellular proteins undergo farnesylation (19), including nuclear laminin A and B, skeletal muscle phosphorylase kinase, and retinal proteins, as well as other members of the Ras superfamily such as Rap2 proteins and RhoB (17, 35–37). Of these, RhoB in particular has been identified as an important putative antineoplastic target of FTIs (38–41). The second observation was initially disappointing in terms of human cancers, because *K-Ras* mutations occur more frequently in human malignancies than *H-Ras* mutations (1). Two factors appear to explain this observation (42). First, K-Ras4B has a 10–20-fold greater affinity for farnesyl protein transferase, the target of FTIs, necessitating much higher levels to inhibit the post-translational processing of this Ras isotype (43). Second, N-Ras, K-Ras4A, and K-Ras4B can also act as substrates for geranylgeranyl protein transferase-1 (43), which catalyzes the addition of a 20-carbon geranylgeranyl isoprenyl group to the cysteine residue of the CAAX motif at the COOH terminal of proteins such as Ras. Under physiological conditions, these Ras isotypes undergo farnesylation almost exclusively, but when treated with FTIs, K- and N-Ras, but not H-Ras, can be efficiently geranylgeranylated

(31), providing an alternative pathway for their post-translational processing.

High-grade astrocytomas do not harbor oncogenic/activating *Ras* mutations (1, 6, 14); however, we have demonstrated that Ras activation does occur in these tumors, attributable in part to overexpression of receptor tyrosine kinases (14). Hence, we have hypothesized that these tumors would be sensitive to growth-inhibition by FTIs. Indeed, we have demonstrated recently (22) that the FTI L-744,832 (Merck Research Laboratories, West Point, PA) inhibits the anchorage-dependent proliferation of five established human malignant astrocytoma cells through a combination of p53-independent G_1-S and G_2-M cell cycle arrest and apoptosis. Furthermore, L-744,832 inhibited the secretion of VEGF, suggesting a further effect of FTIs *in vivo* (16, 22). Other investigators (44) have demonstrated similar results using FTI-276 against U87 cells in an intracranial model. Although these studies serve to demonstrate that FTIs appear capable of inhibiting the growth of astrocytoma cell lines, these and other studies using other human tumor types have not established a causal relationship between Ras activation and drug efficacy. In the present study, we have evaluated the candidate clinical compound SCH66336 (45) to determine its efficacy against astrocytomas and to further our understanding of the relationship of Ras activation and FTIs in human cancers.

Consistent with our previous studies (14) with L-744,832, SCH66336 was capable of inhibiting the growth of established human astrocytoma cell lines, none of which harbor oncogenic *Ras* mutations. However, not all of the cell lines were sensitive, with IC_{50} ranging from 0.6 μM in SF767 cells to 32.3 μM in U373 cells. Furthermore, SCH66336 was effective in inhibiting the growth of two of the three human GBM explant xenografts grown in NOD-SCID mice. Total Ras·GTP levels were not predictive of drug efficacy in either the cell lines or the xenograft models; however, this should not be meant to imply that Ras is not a therapeutic target, because isotype-specific Ras·GTP levels were highly predictive of FTI efficacy. In malignant astrocytomas, cell lines, and specimens, FTIs preferentially inhibited the viability/growth of cells/tumors, in which a large amount of the aberrant growth-promoting signals was being transduced through activation of H-Ras. This finding is entirely consistent with the known pharmacodynamics of FTIs, as discussed above, and demonstrates that high levels of H-Ras·GTP, when combined with low levels of K-Ras·GTP and N-Ras·GTP, are predictive of drug efficacy, even in the absence of oncogenic *Ras* mutations.

Levels of RhoB were measured in the astrocytoma lines and GBM xenografts, because this farnesylated small G-protein has been implicated in transformation and appears to be a major therapeutic target of FTIs. Although we did not measure RhoB activity, expression levels measured by a RhoB-specific antibody on Western blot analysis were not predictive of drug efficacy, unlike the isotype-specific Ras·GTP levels (data not shown). In particular, SF767 (sensitive) and U373 (resistant) cell lines express similar levels of RhoB, and XEN01 (resistant) and XEN08 (sensitive) xenografts express similar levels of RhoB (data not shown). Therefore, our findings in astrocytomas provide compelling evidence that H-Ras is a major therapeutic target of FTIs in human malignancies and that isotype-specific Ras·GTP levels may be a promising diagnostic tool in predicting drug efficacy. Such assays would improve on the current practice of evaluating FTI efficacy through evaluation of inhibition of prelamin A farnesylation in buccal mucosa cells (46, 47) or in peripheral blood mononuclear cells (48) as a surrogate marker of drug efficacy. Finally, our study demonstrates that the lack of activating *Ras* mutations is not an appropriate exclusion criterion for clinical trials of FTIs and that these agents may be useful in the management of tumors such as malignant human astrocytomas.

ACKNOWLEDGMENTS

We thank Dr. W. Robert Bishop (Schering-Plough Research Institute, Kenilworth, NJ) for providing the SCH66336 agent.

REFERENCES

1. Bos, J. L. *ras* oncogenes in human cancers: a review. Cancer Res., *49:* 4682–4689, 1989.
2. Downward, J. Regulation of p21ras by GTPase activating proteins and guanine nucleotide exchange proteins. Curr. Opin. Genet. Dev., *2:* 13–18, 1992.
3. Xu, G. F., O'Connell, P., Viskochil, D., Cawthon, R., Robertson, M., Culver, M., Dunn, D., Stevens, J., Gesteland, R., White, R., and Weiss, R. The neurofibromatosis type 1 gene encodes a protein related to GAP. Cell, *62:* 599–608, 1990.
4. Barbacid, M. Ras genes. Annu. Rev. Biochem., *56:* 779–827, 1987.
5. Smith, M. R., DeGudicibus, S. J., and Stacey, D. W. Requirement for c-ras proteins during viral oncogene transformation. Nature (Lond.), *320:* 540–543, 1986.
6. Tuzi, N. L., Uenter, D. J., Kumar, S., Staddon, S. L., Lemoine, N. R., and Gullick, W. J. Expression of growth factor receptors in human brain tumours. Br. J. Cancer, *63:* 227–233, 1991.
7. Libermann, T. A., Razon, N., Bantal, A. D., Yarden, Y., Schlessinger, J., and Soreq, H. Expression of epidermal growth factor receptors in human brain tumors. Cancer Res., *44:* 753–760, 1984.
8. Steck, P. A., Lee, P., Hung, M. C., and Yung, W. K. Expression of an altered epidermal growth factor receptor by human glioblastoma cells. Cancer Res., *48:* 5433–5439, 1988.
9. Sugawa, N., Ekstrand, A. J., James, C. D., and Collins, V. P. Identical splicing of aberrant epidermal growth factor receptor transcripts from amplified rearranged genes in human glioblastomas. Proc. Natl. Acad. Sci. USA, *87:* 8602–8606, 1990.
10. Wong, A. J., Ruppert, J. M., Bigner, S. H., Grzeschik, C. H., Humphrey, P. A., Bigner, D. S., and Vogelstein, B. Structural alterations of the epidermal growth factor receptor gene in human gliomas. Proc. Natl. Acad. Sci. USA, *89:* 2965–2969, 1992.
11. Fleming, T. P., Saxena, A., Clark, W. C., Robertson, J. T., Oldfield, E. H., Aaronson, S. A., and Ali, I. U. Amplification and/or overexpression of platelet-derived growth factor receptors and epidermal growth factor receptor in human glial tumors. Cancer Res., *52:* 4550–4553, 1992.
12. Nistér, M., Libermann, T. A., Betsholtz, C., Pettersson, M., Claesson-Welsh, L., Heldin, C. H., Schlessinger, J., and Westermark, B. Expression of messenger RNAs for platelet-derived growth factor and transforming growth factor-α and their receptors in human malignant glioma cell lines. Cancer Res., *48:* 3910–3918, 1988.
13. Guha, A., Dashner, K., Black, P. M., Wagner, J. A., and Stiles, C. D. Expression of PDGF and PDGF receptors in human astrocytoma operative specimens supports the existence of an autocrine loop. Int. J. Cancer, *60:* 168–173, 1995.
14. Guha, A., Feldkamp, M. M., Lau, N., Boss, G., and Pawson, A. Proliferation of human malignant astrocytomas is dependent on ras activation. Oncogene, *15:* 2755–2765, 1997.
15. Feldkamp, M. M., Lala, P., Lau, N., Roncari, L., and Guha, A. Expression of activated epidermal growth factor receptors, ras-guanosine triphosphate, and mitogen-activated protein kinase in human glioblastoma multiforme specimens. Neurosurgery (Baltim), *45:* 1442–1453, 1999.
16. Feldkamp, M. M., Lau, N., Rak, J., Kerbel, R. S., and Guha, A. Normoxic and hypoxic regulation of vascular endothelial growth factor (VEGF) by astrocytoma cells is mediated by ras. Int. J. Cancer, *81:* 118–124, 1999.
17. Gibbs, J. B., Oliff, A., and Kohl, N. E. Farnesyltransferase inhibitors: ras research yields a potential cancer therapeutic. Cell, *77:* 175–178, 1994.
18. Hancock, J. F., Paterson, H., and Marshall, C. J. A polybasic domain or palmitoylation is required in addition to the CAAX motif to localize p21ras to the plasma membrane. Cell, *63:* 133–139, 1990.
19. Marshall, C. J. Protein prenylation: a mediator of protein-protein interactions. Science (Wash. DC), *259:* 1865–1866, 1993.
20. Nagasu, T., Yoshimatsu, K., Rowell, C., Lewis, M. D., and Garcia, A. M. Inhibition of human xenograft growth by treatment with the farnesyl transferase inhibitor B956. Cancer Res., *55:* 5310–5314, 1995.
21. Sepp-Lorenzino, L., Ma, Z., Rands, E., Kohl, N. E., Gibbs, J. B., Oliff, A., and Rosen, N. A peptidomimetic inhibitor of farnesyl: protein transferase blocks the anchorage-dependent and -independent growth of human tumor cell lines. Cancer Res., *55:* 5302–5309, 1995.
22. Feldkamp, M. M., Lau, N., and Guha, A. Growth inhibition of astrocytoma cells by farnesyl transferase inhibitors is mediated by a combination of antiproliferative, pro-apoptotic, and anti-angiogenic effects. Oncogene, *18:* 7514–7526, 1999.
23. Adjei, A. A., Erlichman, C., Davis, J. N., Cutler, D. L., Sloan, J. A., Marks, R. S., Hanson, L. J., Svingen, P. A., Atherton, P., Bishop, W. R., Kirschmeier, P., and Kaufmann, S. H. A Phase I trial of the farnesyl transferase inhibitor SCH66336: evidence for biological and clinical activity. Cancer Res., *60:* 1871–1877, 2000.
24. Liu, M., Bryant, M. S., Chen, J., Lee, S., Yaremko, B., Li, Z., Dell, J., Lipari, P., Malkowski, M., Prioli, N., Rossman, R. R., Korfmacher, W. A., Nomeir, A. A., Lin, C. C., Mallams, A. K., Doll, R. J., Catino, J. J., Girijavallabhan, V. M., Kirschmeier, P., and Bishop, W. R. Effects of SCH 59228, an orally bioavailable farnesyl protein transferase inhibitor, on the growth of oncogene-transformed fibroblasts and a human colon carcinoma xenograft in nude mice. Cancer Chemother. Pharmacol., *43:* 50–58, 1999.
25. Liu, M., Bryant, M. S., Chen, J., Lee, S., Yaremko, B., Lipari, P., Malkowski, M., Ferrari, E., Nielsen, L., Prioli, N., Dell, J., Sinha, D., Syed, J., Korfmacher, W. A., Nomeir, A. A., Lin, C. C., Wang, L., Taveras, A. G., Doll, R. J., Njoroge, F. G., Mallams, A. K., Remiszewski, S., Catino, J. J., Girijavallabhan, V. M., Bishop, W. R.,

et al. Antitumor activity of SCH 66336, an orally bioavailable tricyclic inhibitor of farnesyl protein transferase, in human tumor xenograft models and wap-Ras transgenic mice. Cancer Res., *58:* 4947–4956, 1998.
26. Taveras, A. G., Deskus, J., Chao, J., Vaccaro, C. J., Njoroge, F. G., Vibulbhan, B., Pinto, P., Remiszewski, S., del Rosario, J., Doll, R. J., Alvarez, C., Lalwani, T., Mallams, A. K., Rossman, R. R., Afonso, A., Girijavallabhan, V. M., Ganguly, A. K., Pramanik, B., Heimark, L., Bishop, W. R., Wang, L., Kirschmeier, P., James, L., Carr, D., Liu, M., *et al.* Identification of pharmacokinetically stable 3, 10-dibromo-8-chlorobenzocycloheptapyridine farnesyl protein transferase inhibitors with potent enzyme and cellular activities. J. Med. Chem., *42:* 2651–2661, 1999.
27. Goodwin, C. J., Holt, S. J., Downes, S., and Marshall, N. J. Microculture tetrazolium assays: a comparison between two new tetrazolium salts. XTT and MTS. J. Immunol. Methods, *179:* 95–103, 1995.
28. Gavrieli, Y., Sherman, Y., and Ben-Sasson, S. A. Identification of programmed cell death *in situ* via specific labeling of nuclear DNA fragmentation. J. Cell Biol., *119:* 493–501, 1992.
29. Scheele, J. S., Rhee, J. M., and Boss, G. R. Determination of absolute amounts of ras GDP and GTP bound to ras in mammalian cells: comparison of parental and ras-overproducing NIH 3T3 fibroblasts. Proc. Natl. Acad. Sci. USA, *92:* 1097–1100, 1994.
30. Guha, A., Lau, N., Huvar, I., Gutmann, D., Provias, J., Pawson, T., and Boss, G. Ras-GTP levels are elevated in human NF1 peripheral nerve tumors. Oncogene, *12:* 507–513, 1996.
31. Whyte, D. B., Kirschmeier, P., Hockenberry, T. N., Nunez-Oliva, I., James, L., Catino, J. J., Bishop, W. R., and Pai, J. K. K- and N-Ras are geranylgeranylated in cells treated with farnesyl protein transferase inhibitors. J. Biol. Chem., *272:* 14459–14464, 1997.
32. Gibbs, J. B. Ras C-terminal processing enzymes–new drug targets? Cell, *65:* 1–4, 1991.
33. Reiss, Y., Goldstein, J. L., Seabra, M. C., Casey, P. J., and Brown, M. S. Inhibition of purified p21ras farnesyl: protein transferase by Cys-AAX tetrapeptides. Cell, *62:* 81–88, 1990.
34. James, G., Goldstein, J. L., and Brown, M. S. Resistance of K-RasBV12 proteins to farnesyltransferase inhibitors in Rat1 cells. Proc. Natl. Acad. Sci. USA, *93:* 4454–4458, 1996.
35. James, G. L., Goldstein, J. L., Brown, M. S., Rawson, T. E., Somers, T. C., McDowell, R. S., Crowley, C. W., Lucas, B. K., Levinson, A. D., and Marsters, J. C., Jr. Benzodiazepine peptidomimetics: potent inhibitors of ras farnesylation in animal cells. Science (Wash. DC), *260:* 1937–1942, 1993.
36. Moores, S. L., Schaber, M. D., Mosser, S. D., Rands, E., O'Hara, M. B., Garsky, V. M., Marshall, M. S., Pompliano, D. L., and Gibbs, J. B. Sequence dependence of protein isoprenylation. J. Biol. Chem., *266:* 14603–14610, 1991.
37. Farrell, F. X., Yamamoto, K., and Lapetina, E. G. Prenyl group identification of rap2 proteins: a ras superfamily member other than ras that is farnesylated. Biochem. J., *289:* 349–355, 1993.
38. Lebowitz, P. F., Davide, J. P., and Prendergast, G. C. Evidence that farnesyltransferase inhibitors suppress ras transformation by interfering with Rho activity. Mol. Cell. Biol., *15:* 6613–6622, 1995.
39. Lebowitz, P. F., Sakamuro, D., and Prendergast, G. C. Farnesyl transferase inhibitors induce apoptosis of ras-transformed cells denied substratum attachment. Cancer Res., *57:* 708–713, 1997.
40. Lebowitz, P. F., Du, W., and Prendergast, G. C. Prenylation of RhoB is required for its cell transforming function but not its ability to activate serum response element-dependent transcription. J. Biol. Chem., *272:* 16093–16095, 1997.
41. Du, W., Lebowitz, P. F., and Prendergast, G. C. Cell growth inhibition by farnesyltransferase inhibitors is mediated by gain of geranylgeranylated RhoB. Mol. Cell. Biol., *19:* 1831–1840, 1999.
42. Fiordalisi, J. J., Rushton, B. C., Toussaint, L. G., III, Johnson, R. L., II, and Cox, A. D. High affinity for FTase and alternative prenylation contribute individually to K-Ras resistance to FTIs. Proc. Am. Assoc. Cancer Res., *40:* 34–39, 1999.
43. Zhang, F. L., Kirschmeier, P., Carr, D., James, L., Bond, R. W., Wang, L., Patton, R., Windsor, W. T., Syto, R., Zhang, R., and Bishop, W. R. Characterization of Ha-Ras, N-Ras, Ki-Ras4A, and Ki-Ras4B as *in vitro* substrates for farnesyl protein transferase and geranylgeranyl protein transferase type I. J. Biol. Chem., *272:* 10232–10239, 1997.
44. Pollack, I. F., Bredel, M., Erff, M., Hamilton, A. D., and Sebti, S. M. Inhibition of ras and related guanosine triphosphate-dependent proteins as a therapeutic strategy for blocking malignant glioma growth: II–preclinical studies in a nude mouse model. Neurosurgery (Baltim), *45:* 1208–1215, 1999.
45. Njoroge, F. G., Taveras, A. G., Kelly, J., Remiszewski, S., Mallams, A. K., Wolin, R., Afonso, A., Cooper, A. B., Rane, D. F., Liu, Y. T., Wong, J., Vibulbhan, B., Pinto, P., Deskus, J., Alvarez, C. S., del Rosario, J., Connolly, M., Wang, J., Desai, J., Rossman, R. R., Bishop, W. R., Patton, R., Wang, L., Kirschmeier, P., Ganguly, A. K., *et al.* (+)-4-[2-[4-(8-Chloro-3,10-dibromo-6,11-dihydro-5H-benzo[5,6]-cyclohepta[1,2-b]-pyridin-11(R)-yl)-1-piperidinyl]-2-oxo-ethyl]-1-piperidinecarboxamide (SCH-66336): a very potent farnesyl protein transferase inhibitor as a novel antitumor agent. J. Med. Chem., *41:* 4890–4902, 1998.
46. Adjei, A. A., Erlichman, C., Davis, J. N., Reid, J., Sloan, J., Statkevich, P., Zhu, Y., Marks, R. S., Pitot, H. C., Goldberg, R., Hanson, L., Alberts, S., Cutler, D., and Kaufmann, S. H. A Phase I and pharmacologic study of the farnesyl protein transferase (FPT) inhibitor SCH 66336 in patients with locally advanced or metastatic cancer. Proc. Annu. Meet. Am. Soc. Clin. Oncol., *1999:* 598, 1999.
47. Awada, A., Eskens, F., Piccart, M. J., van der Gaast, A., Bleiberg, H., Cutler, D. L., Fumoleau, P., Wanders, J., Faber, M. N., and Verweij, J. A clinical, pharmacodynamic, and pharmacokinetic Phase I study of SCH 66336 (SCH), an oral inhibitor of the enzyme farnesyl transferase given once daily in patients with solid tumors. Clin. Cancer Res., *5* (Suppl.)*:* 20, 1999.
48. Hurwitz, H. I., Colvin, O. M., Petros, W. P., Williams, R., Conway, D., Adams, D. J., Casey, P. J., Calzetta, A., Mastorides, P., Statkevich, P., and Cutler, D. Phase I and pharmacokinetic study of SCH66336, a novel FPTI, using a 2-week on, 2-week off schedule. Proc. Annu. Meet. Am. Soc. Clin. Oncol., *1999:* 599, 1999.
49. Lehman, A., and Sall, J. JMP Statistics and Graphics Guide, Version 3. Cary, NC: SAS Institute, 1995.